HEAT GENERATION IN AIRCRAFT TIRES

Samuel K. Clark
University of Michigan

ABSTRACT

A method has been developed for calculating the internal temperature distribution in an aircraft tire while free rolling under load. The method uses an approximate stress analysis of each point in the tire as it rolls through the contact patch. From this stress change, the mechanical work done on each volume element may be obtained and converted into a heat release rate through a knowledge of material characteristics. The tire cross-section is then considered as a body with internal heat generation, and the diffusion equation is solved numerically with appropriate boundary conditions of the wheel and runway surface. Comparison with data obtained with buried thermocouples in tires shows good agreement. The data presented in this paper were excerpted from reference 1.

The origin of aircraft tire heating lies in the hysteretic loss characteristics of polymeric materials used for both the nylon textile cord reinforcement and for the rubber components in an aircraft tire. Figure 1 shows a typical stress-strain curve between the two end points of the cyclic stress states associated with rolling a material element through the contact patch of the tire and out again.

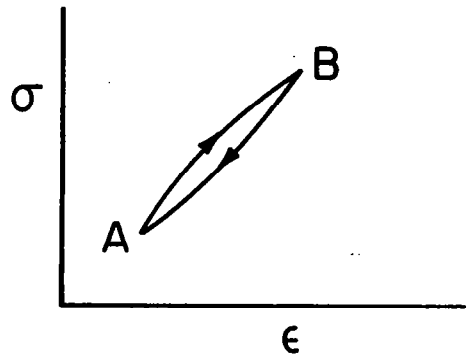

Figure 1

The stress excursion is presumed to occur between two points A and B located 180° apart on the rolling tire. One extreme is the upper point A where only inflation pressures act to produce an axisymmetric stress state of the tire. The other extreme point is the center of the contact patch, where again an axisymmetric solution is used to obtain the stress state in the tire deformed against a flat surface (fig. 2).

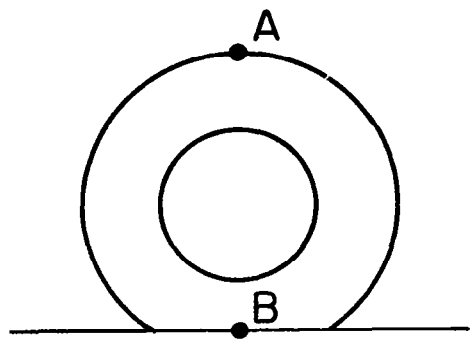

Figure 2

Figure 3 illustrates the assumed conditions in the vicinity of the contact patch of the tire. A total deflection Δ is presumed to take place between the outer surface of the tire crown and the ground. Inside this contact patch region the tire is presumed to be in complete contact with the flat runway surface.

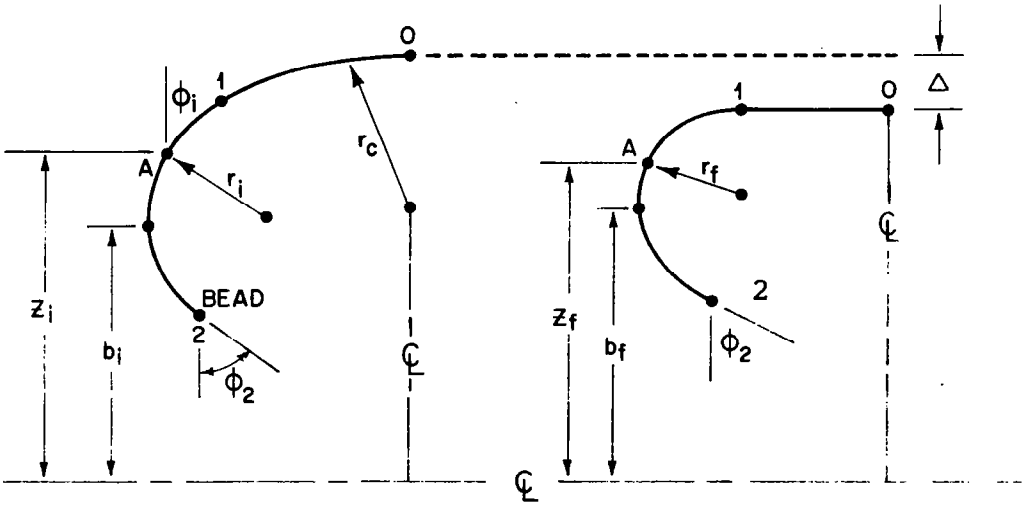

(a) Assumed geometry at point A of figure 2.

(b) Assumed geometry at point B of figure 2.

Figure 3

Figure 4 shows the assumed geometry of the tire at the two extreme conditions A and B illustrated in figures 2 and 3. In the case of axisymmetric inflation loads the geometric midline of the tire is represented by a torus as shown. For that portion of the tire in the center of the contact patch, the shape is considered to be flat in the contact region and made up of a single circular arc outside the contact region. The stress solutions are both obtained from axisymmetric considerations.

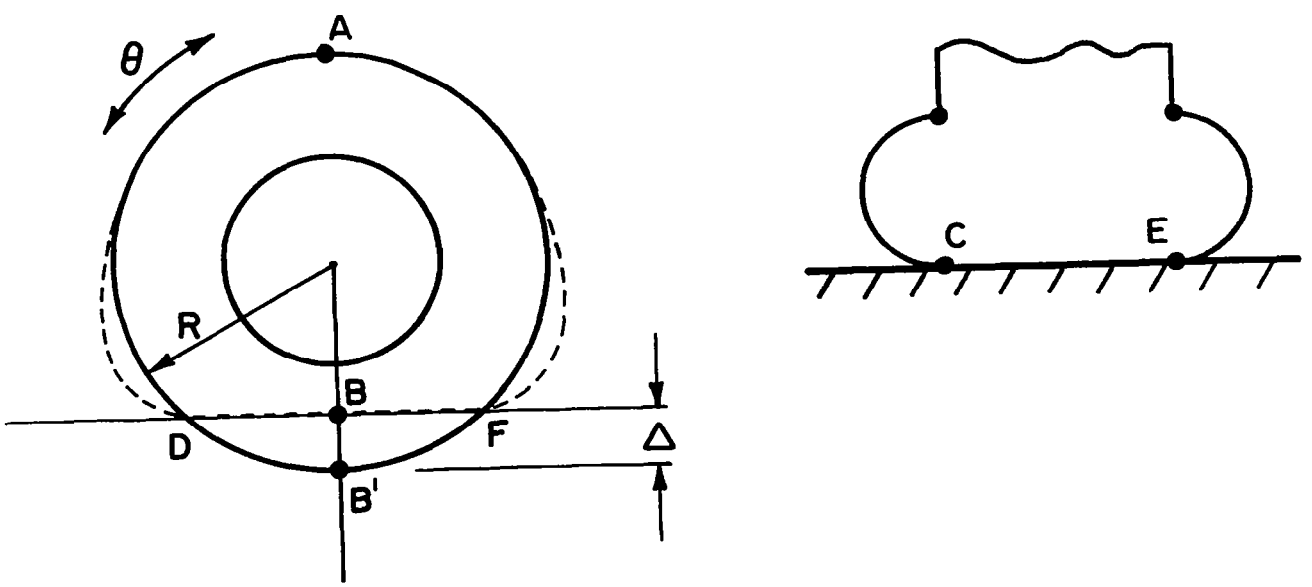

Figure 4

The tire is divided into five segments for purposes of both stress and thermal analysis (fig. 5). Segment I is that portion of the tire carcass lying in the contact patch. It has plane orthotropic elastic properties. Segment II is isotropic tread material in contact with the runway surface, and hence is acted upon by normal pressures as well as by membrane and bending strains. Segment III is that part of the side wall acted on by internal pressure, and also has orthotropic elastic properties. Segment IV is the sidewall cover of the tire and is considered to be isotropic in its material properties. Segment V is the bead region which is subject to a special description.

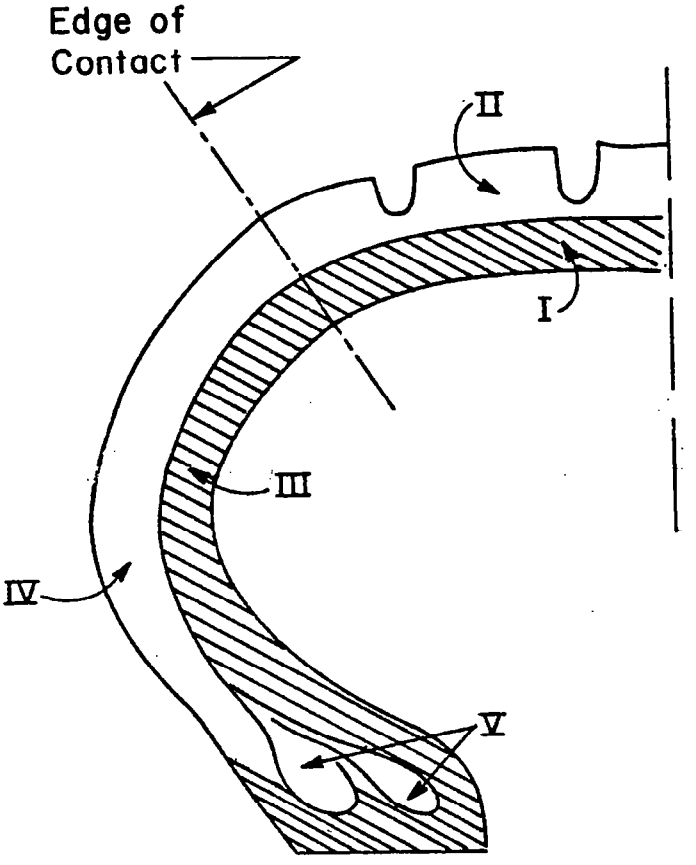

Figure 5

Figure 6 shows the method of splitting the tire cross section into various rectangular segments for purposes of thermal analysis. In general the decomposition process follows the natural boundary lines of the tire between the orthotropic and isotropic regions.

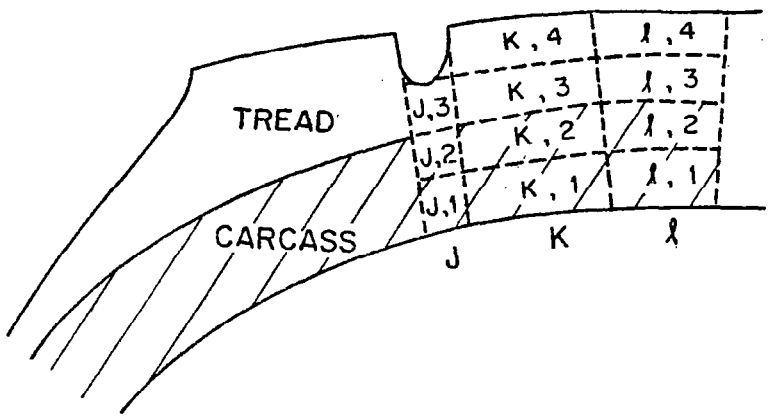

Figure 6

Figure 7 is the general heat diffusion equation which is being modeled on a discrete basis in the numerical calculation described here. However, the elements which are in contact with the outer surface or with the bead area of the tire have additional terms associated with either thermal conduction into the metallic wheel or convective heat transfer loss to the air.

$$K \nabla^2 \theta = \rho \frac{\partial \theta}{\partial t} - \dot{q}$$

where

K = thermal conductivity

ρ = density

$\dot{q}$ = heat generation rate

θ = temperature

Figure 7

The equation for convective heat transfer, temperature buildup and internal heat generation is discretized into the form shown in figure 8 for numerical calculation throughout the tire cross section. Note that due to the higher rotational speeds of the tire compared to thermal diffusion times, the temperature distribution is completely axisymmetric.

$$\frac{\Delta\theta}{\Delta t} = \dot{q} + \bar{\alpha}_{K-1,K,\ell}\,(\theta_{K-1,\ell} - \theta_{K,\ell}) + \bar{\alpha}_{K,K+1,\ell}\,(\theta_{K+1,\ell} - \theta_{K,\ell}) + \bar{\alpha}_{K,\ell-1,\ell}\,(\theta_{K,\ell-1} - \theta_{K,\ell}) + \bar{\alpha}_{K,\ell,\ell+1}\,(\theta_{K,\ell+1} - \theta_{K,\ell})$$

with

$$\bar{\alpha}_{l,m,n} = \frac{KA}{d}$$

K = thermal conductivity

A = area of contact between subscripted elements

d = distance between centroids of subscripted elements

NOTATION FOR THERMAL ELEMENTS

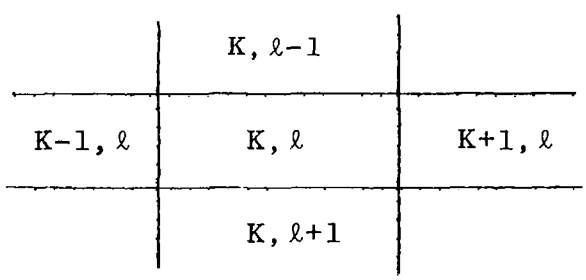

Figure 8

The strain energy density must be related to the hysteretic loss, which results in internal heat generation. Due to the lack of appropriate material constants, this is now being done on a provisional basis using the loss tangent tan δ, a quantity usually associated with uniaxial sinusoidal loading. Due to the linear relationship between rate of heat generation and frequency, the rate of heat generation is linearly proportional to aircraft velocity (fig. 9).

$$\dot{q} \cong 0.01 \frac{UV_o \tan\delta}{r_o - \Delta/3} \text{ cal/cm}^3\text{/sec}$$

where r_o = outside radius of tire, in.

Δ = tire deflection, in.

V_o = aircraft velocity, ft/sec

U = elastic energy, in.-lb/in.^{3}

Figure 9

In data shown in subsequent figures, calculations are carried out comparing predictions of this program with measured temperature rise data. These predictions are based on best estimates of material properties taken from the literature (ref. 2). These are given in figure 10.

MATERIAL CHARACTERISTICS OF

22 x 5.5 and 40 x 14 AIRCRAFT TIRES

Region[a]	Young's modulus of rubber, E, psi	Shear modulus of rubber, G, psi	[b]$\tan\delta_o$, psi	Cord angle, α, deg	Thermal conductivity, K, cal-cm/°C-cm^2-sec	Density, ρ, deg	Specific heat, C_p,
Tread (II)		335	0.15		5×10^{-4}	1.0	0.5
Carcass (I, III)	(c)		0.15	(d)	5×10^{-4}	1.0	0.5
Sidewall rubber (IV)		335	0.15			1.0	0.5
Bead (V)	15×10^6		0.03				

[a]See fig. 5.

[b]Values of $\tan\delta_o$ are given for 25°C. For higher temperatures, $\tan\delta$ is calculated by the approximate expression

$$\tan\delta = \tan\delta_o(e^{-.01\Delta\theta})$$

where $\Delta\theta$ is the temperature rise in °C above ambient.

[c]See reference 1. For shear modulus G of rubber use 335 psi.

[d]Calculated by cosine law using $\alpha = 35°$ crown angle.

Figure 10

Figure 11 represents a cross section of half of the 22 x 5.5 8 PR tire showing the elements used for temperature calculation as well as the thermocouple displacement used in the experimental program.

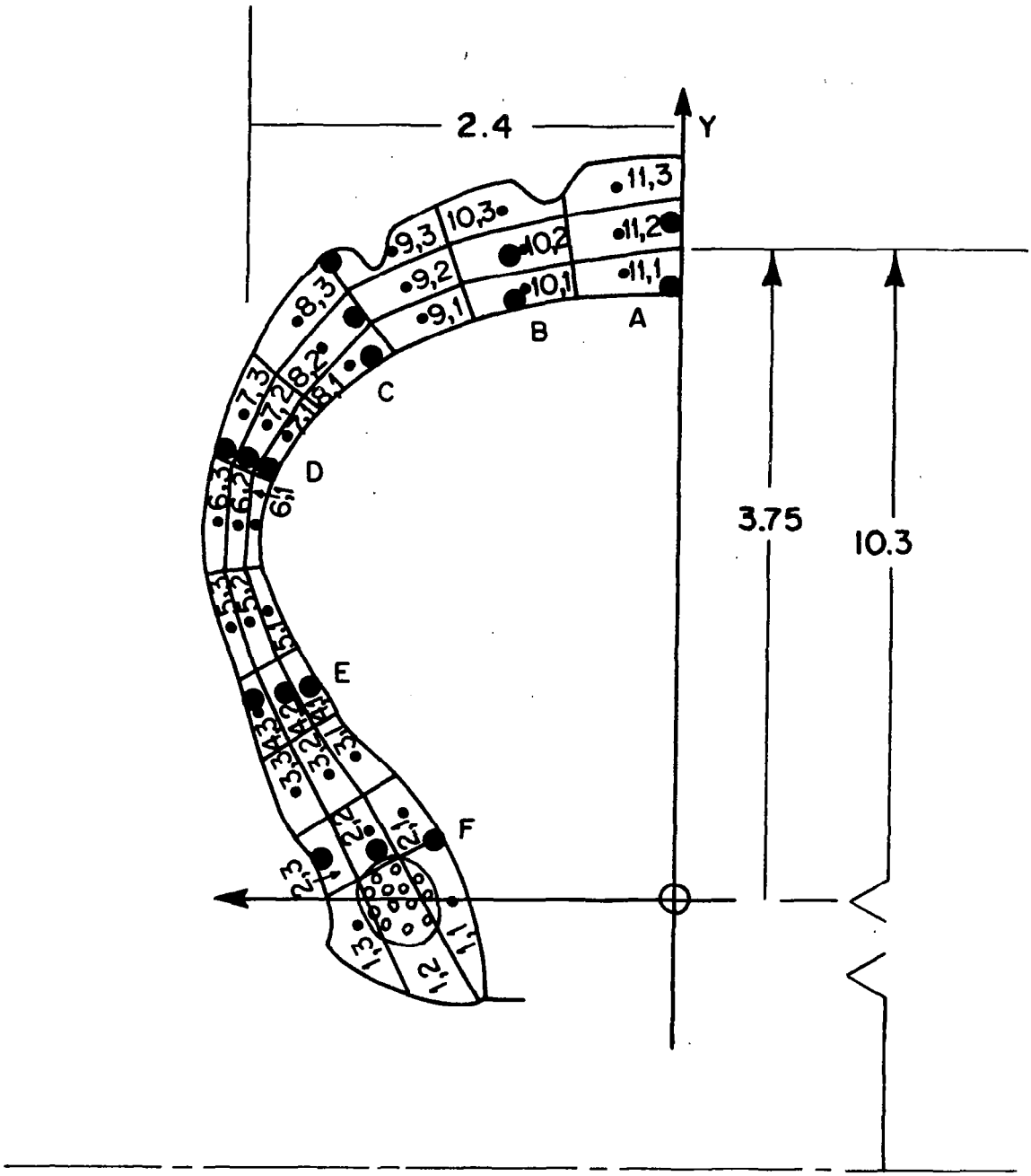

Figure 11

Figure 12 shows comparison between temperature rise and time as measured by thermocouples, along with calculations for similar locations on the tire using the computer program previously described. Stations A through F correspond to those shown in figure 11.

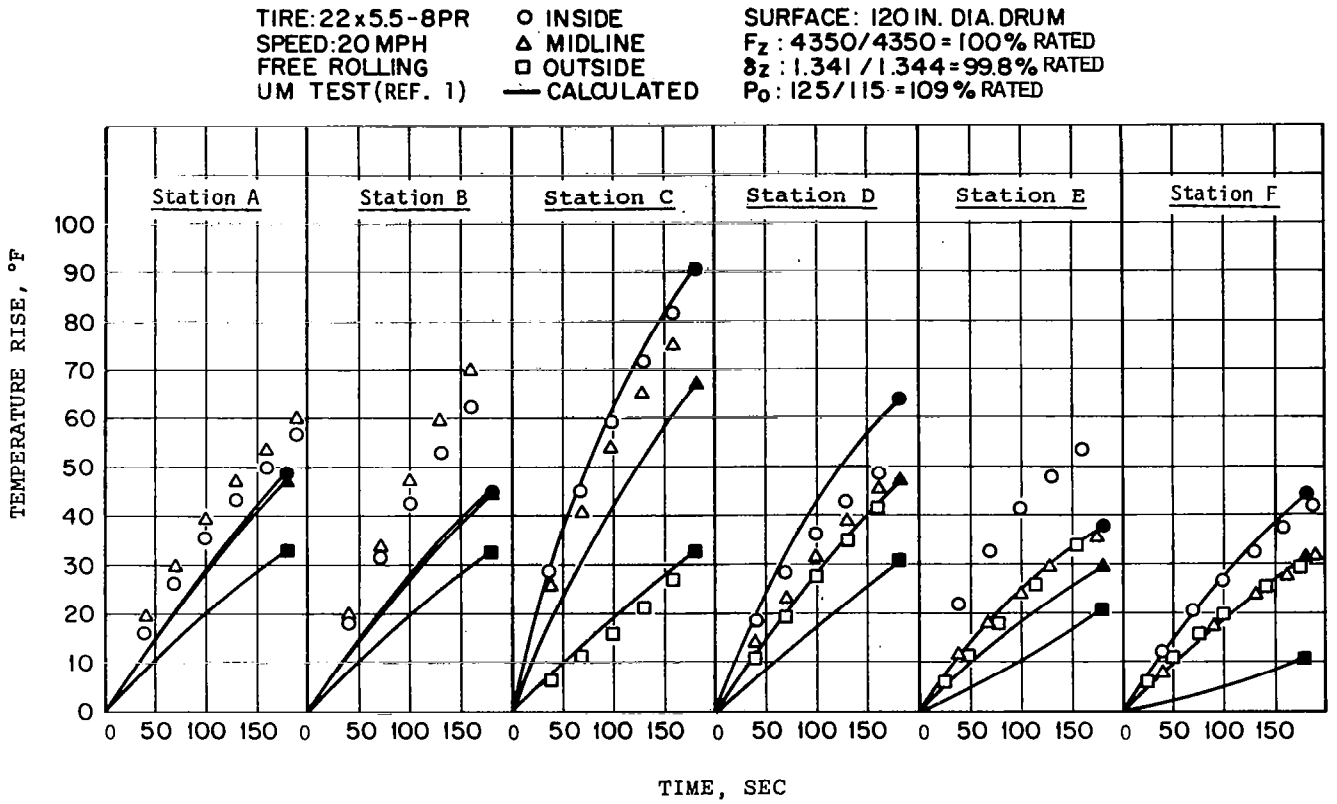

Figure 12

Figure 13 shows similar temperature vs. time information for a different form of this 22 x 5.5 tire. In this case the tire is a 12 PR tire and requires a different geometric description due to the thicker carcass. This in turn results in considerably higher temperatures being generated as this tire is run under rated load conditions for approximately 150 seconds. Again, measured data is compared with calculations from the computer program.

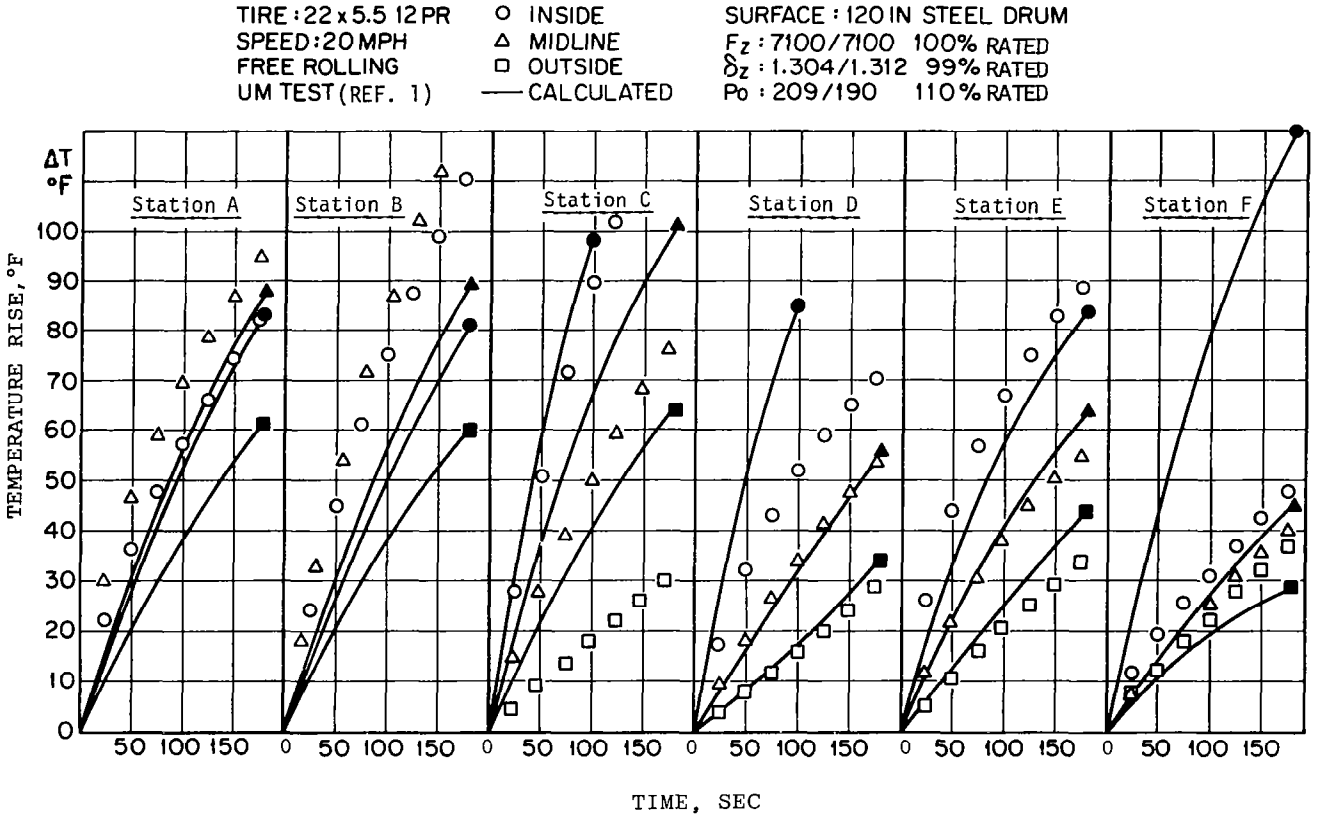

Figure 13

Figure 14 shows a cross section of a 40 x 14 28 PR tire used as a model of a large aircraft tire. This is a common commercial tire, and in this case a larger number of discrete sections is chosen for temperature calculation purposes. Again, thermocouple locations are shown by the black dots. Extensive experimental work has been done on this tire in order to compare it with the calculation.

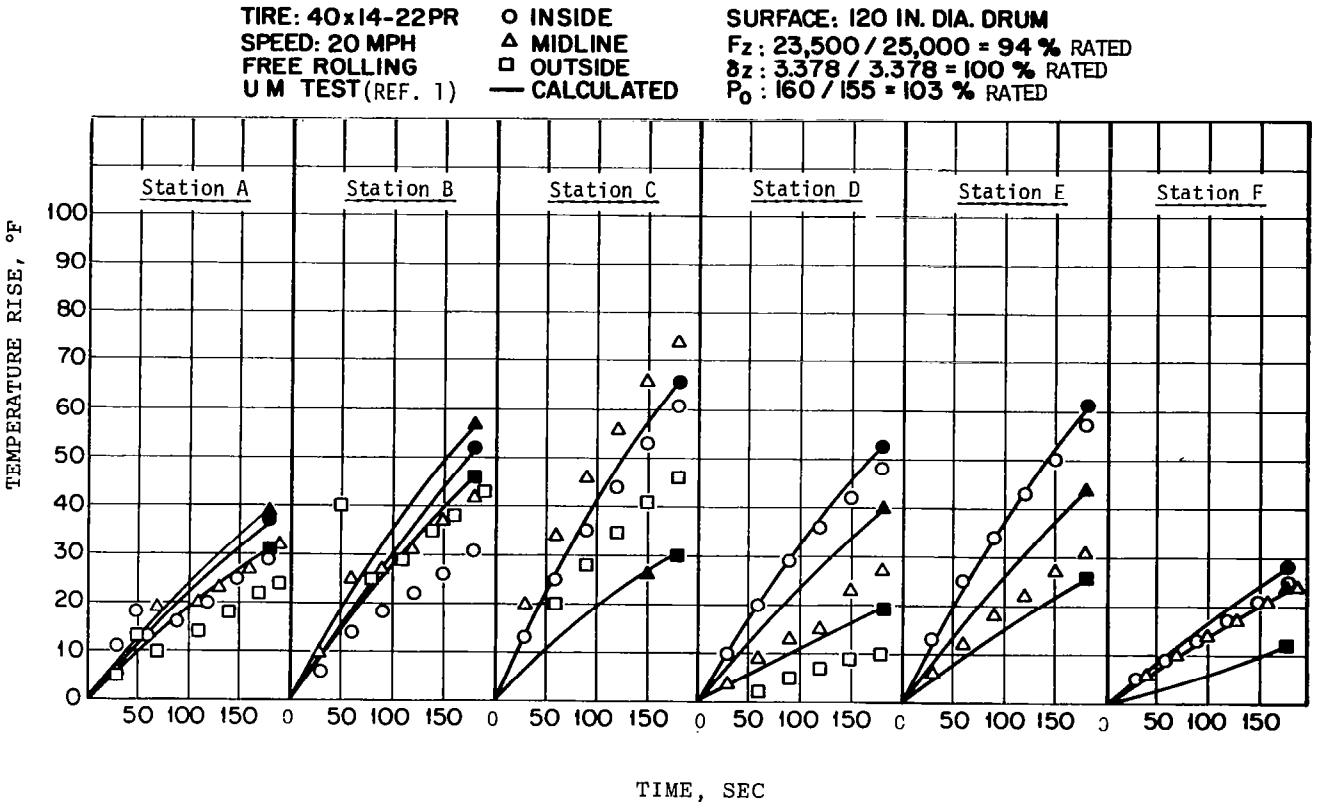

Figure 14

Figure 15 shows a comparison between a 22 ply rated version of the tire shown in figure 14 and calculations carried out using the program described previously. These calculations generally agree will with measured data.

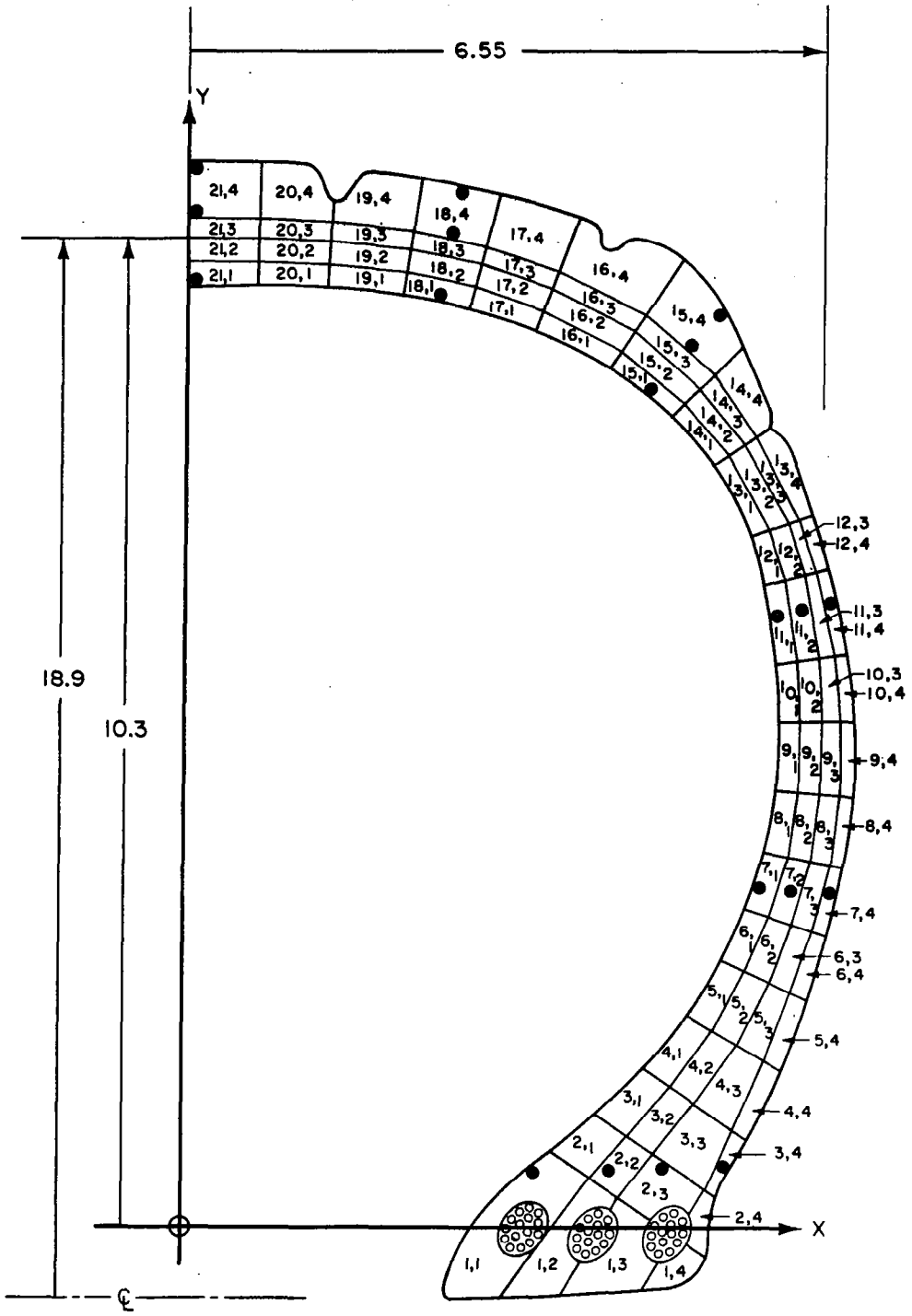

Dimensions in inches

Figure 15

Figure 16 shows temperature rise data up to approximately 150 seconds of running time under essentially rated conditions for the 28 ply rated version of this tire. In this case calculations agree well with experimental measurements, although here the thicker section tire also requires a separate geometric description.

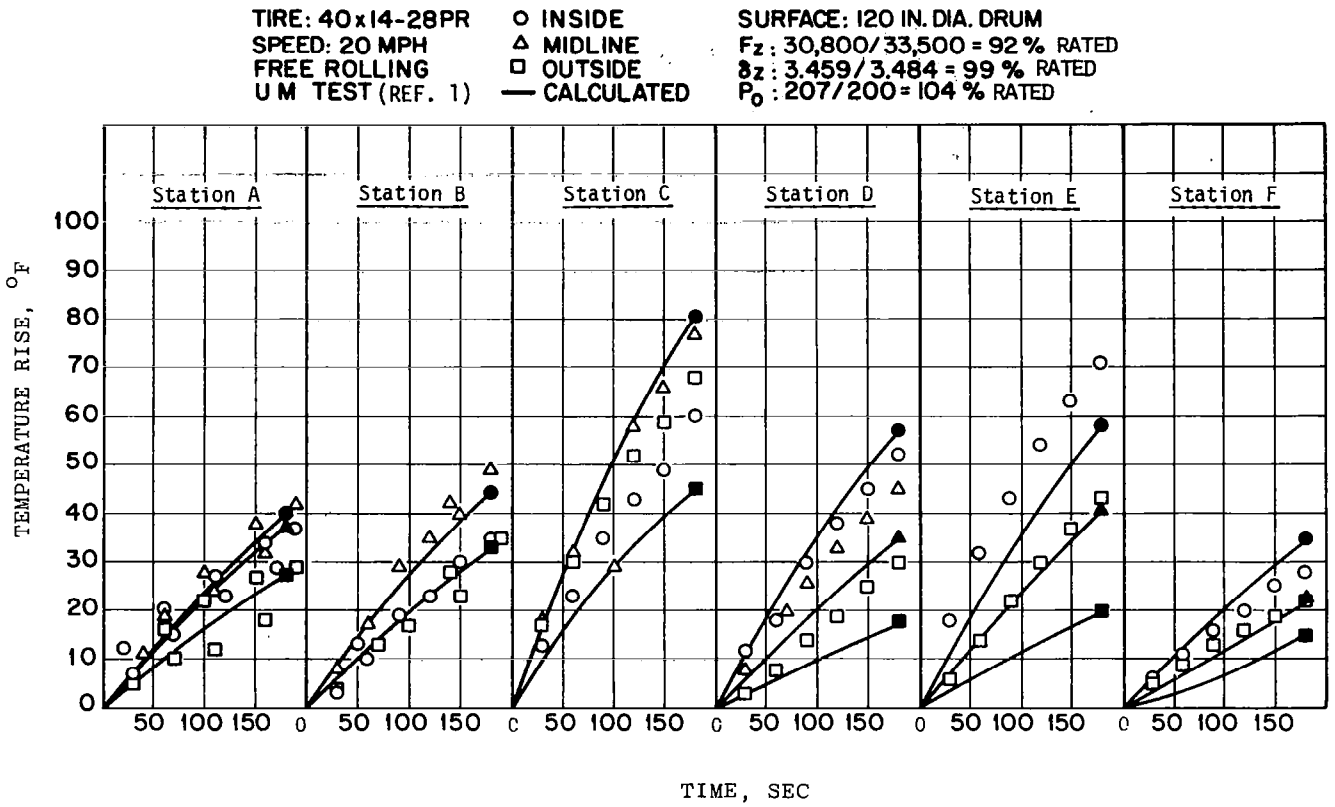

Figure 16

REFERENCE

1. Clark, Samuel K.; and Dodge, Richard N.: Heat Generation in Aircraft Tires Under Free Rolling Conditions. NASA CR-3629, 1982.

2. Clark, S. K. (ed.): Mechanics of Pneumatic Tires, NBS Monograph 122, National Bureau of Standards, 1981.